Flight Research

[redacted]

NASA TM X-257

NASA TM X-257

N-07
34P

TECHNICAL MEMORANDUM

X-257

INTERNAL-PERFORMANCE EVALUATION OF TWO FIXED-DIVERGENT-SHROUD EJECTORS

By James R. Mihaloew

Lewis Research Center
Cleveland, Ohio

NATIONAL AERONAUTICS AND SPACE ADMINISTRATION
WASHINGTON

[redacted]

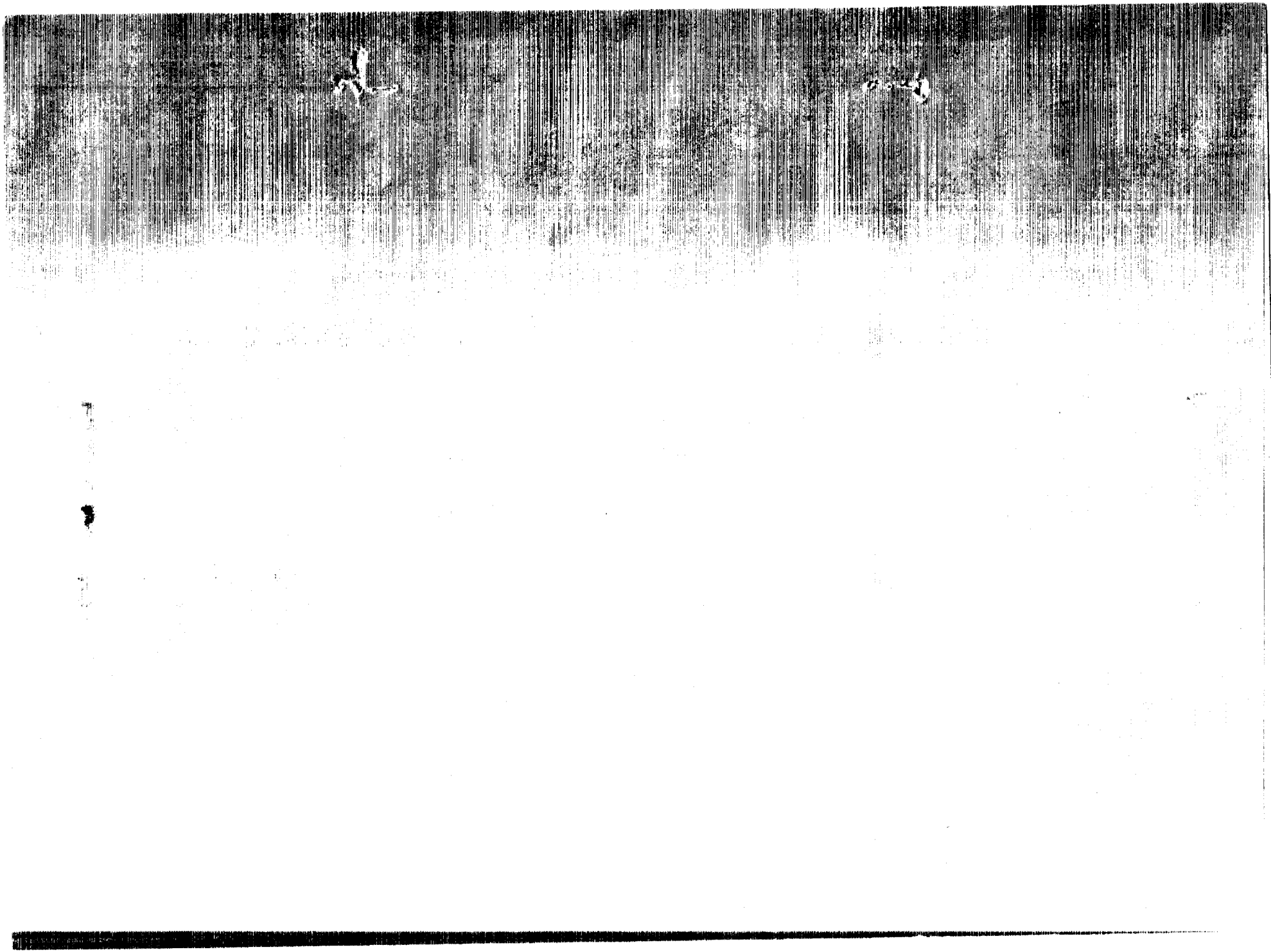

[redacted]

NATIONAL AERONAUTICS AND SPACE ADMINISTRATION

TECHNICAL MEMORANDUM X-257

INTERNAL-PERFORMANCE EVALUATION OF TWO FIXED-DIVERGENT-SHROUD EJECTORS*

By James R. Mihaloew

ABSTRACT

Ejectors designed for use in a Mach 2.2 aircraft were evaluated over a range of representative primary pressure ratios and ejector corrected weight-flow ratios. Basic thrust and pumping characteristics are discussed in terms of an assumed engine operating schedule to illustrate the variation of performance with Mach number. The two designs differed about 16 percent in the shroud longitudinal spacing ratio. For corrected ejector weight-flow ratios up to 0.10, the performance of the fixed-shroud ejector designs is comparable with that of a similar continuously variable ejector except at conditions corresponding to acceleration with afterburning from Mach 0.4 to 1.2. In this region, the ejector thrust ratio decreased to a minimum of 0.96.

INDEX HEADINGS

Nozzles	1.4.2.2
Exits	1.4.3
Pumps, Jet and Thrust Augmentors	1.4.4

*Title, Unclassified.

[redacted]

NATIONAL AERONAUTICS AND SPACE ADMINISTRATION

TECHNICAL MEMORANDUM X-257

INTERNAL-PERFORMANCE EVALUATION OF TWO FIXED-DIVERGENT-SHROUD EJECTORS*

By James R. Mihaloew

SUMMARY

A 0.278-scale quiescent-air internal-performance evaluation was conducted on two fixed-divergent-shroud ejectors designed for operation at flight Mach numbers up to 2.2. The two ejectors differed by about 16 percent in shroud longitudinal spacing ratio and had primary-nozzle positions corresponding to turbojet nonafterburning and afterburning operating conditions. The ejectors were tested with dry unheated air over a range of primary pressure ratios up to 16.0 and ejector corrected weight-flow ratios up to 0.10.

It was determined that, for ejector corrected weight-flow ratios up to 0.10, the ejector will provide internal thrust performance equal to that of continuously variable shroud ejectors (ejector thrust ratios as high as 0.99) except for conditions simulating afterburning acceleration in the Mach number region from 0.4 to 1.2, where the thrust ratio decreased to a minimum of 0.96.

INTRODUCTION

Previous investigations (refs. 1 to 8) have shown that, for flight at high subsonic and low supersonic speeds, convergent and cylindrical fixed-shroud ejectors provide excellent thrust performance and that at higher supersonic speeds a divergent-shroud ejector is necessary to maintain efficient expansion. As aircraft speed is increased, however, the range of conditions over which the ejector must operate is also increased, and off-design problems are encountered. One method of avoiding these off-design problems is to use variable geometry that will provide the desired thrust performance at the expense of mechanical complexity and weight. If, however, the aircraft flight plan is such that the quantity of fuel consumed during the off-design condition is relatively small, a fixed-shroud ejector could possibly be used; and the weight saving and mechanical simplicity may outweigh the somewhat reduced off-design performance.

*Title, Unclassified.

In order to provide information pertinent to this problem, an investigation was conducted to evaluate the internal performance of two fixed-divergent-shroud ejectors over a range of primary pressure ratios and ejector weight-flow ratios applicable to a supersonic aircraft operating at Mach numbers up to 2.2. Each ejector consisted of a fixed 10°-half-angle conical-section divergent shroud and a two-position primary nozzle that simulated nonafterburning and afterburning operation. The two ejector designs differed in longitudinal spacing ratio by about 16 percent. All configurations were tested in a quiescent-air thrust rig using pressurized dry unheated air discharging into an evacuated tank.

The basic thrust and pumping performance of each configuration is presented as a function of primary pressure ratio, and the composite performance is shown in terms of an assumed engine operating schedule. A method of determining internal thrust by momentum and pressure integration (ref. 9) was also applied to the ejector, and a comparison was made with the measured thrust values to determine the validity of such a method for application to full-scale in-flight thrust measurement.

APPARATUS

Ejector

A diagrammatic sketch of the ejectors and values of the ejector dimensional parameters are given in figure 1. Two ejector designs differing in longitudinal spacing were investigated. Both ejectors used a 10°-half-angle conical-section divergent shroud and two fixed primary nozzles that simulated nonafterburning operation (exit diameter ratio, 1.84) and afterburning operation (exit diameter ratio, 1.40). A 1.375-inch spacer was installed at the shroud mounting flange shown in figure 2 to effect the change in longitudinal spacing. The ejectors were designed to provide optimum performance in the simulated afterburning position at a primary pressure ratio of about 12.0 which, in the assumed flight plan, would occur at a Mach number of 2.2. The simulated nonafterburning configurations were designed to induce separation at primary pressure ratios up to about 4.0 in order to avoid overexpansion losses and provide performance similar to a convergent nozzle. In the transition from nonafterburning to afterburning, the primary-nozzle exit would translate upstream.

Test Setup

The ejectors were installed in the test setup as shown schematically in figure 3. The setup consisted of a plenum chamber, mounted between the laboratory high-pressure-air and altitude-exhaust systems, that

contained a bedplate freely suspended by four flexure rods on which the ejector and mounting pipe were installed. Two labyrinth seals installed in series upstream of the mounting pipe maintained the pressure difference between the inlet air and exhaust systems. The resultant force on the ejector and mounting pipe produced by internal and external pressures was transmitted through a thrust linkage to a calibrated null-type pressure force-measuring cell. The facility is the same as described in other ejector reports (e.g., ref. 7).

Instrumentation

Instrumentation stations and details are indicated in figures 2 and 3, and the description and use are given in the following table:

Station	Location	Static-pressure taps	Total-pressure tubes	Temperature thermocouples	Use
0	Ambient	4	--	-	Ambient in tank
1	Inlet	-	--	2	Primary-inlet momentum
2	Forward bellmouth	4	--	-	Primary-inlet momentum
3	Primary-air measuring	4	12 (2 rakes)	-	Primary mass flow
4	Rear bellmouth	4	--	-	External pressure force
5	Upstream secondary orifice	1	--	2	Secondary mass flow
6	Downstream secondary orifice	1	--	-	Secondary mass flow
7	Thrust cell	-	1	-	Resultant force
p	Primary inlet	4	8 (1 rake)	2	Primary-nozzle inlet condition
s	Secondary inlet	8	6 (2 rakes)	2	Integrated thrust
d	Divergent shroud	12	--	-	

PROCEDURE

Dry unheated air at approximately 3000 pounds per square foot absolute was used in this investigation. Prior to running the ejector configurations, the performance of each primary nozzle was evaluated over a range of primary pressure ratios from 1.5 to 18.0 to determine the primary exit momentum for the integrated thrust method. For the ejector

configurations, a range of primary pressure ratios from 2.0 to approximately 18.0 was covered in increasing and decreasing order at ejector corrected weight-flow ratios of 0 to 0.08 for the nonafterburning configurations and 0 to 0.10 for the afterburning configurations. The ejector corrected weight-flow ratio $(w_s/w_p)\sqrt{T_s/T_p}$ with $\sqrt{T_s/T_p} = 1.0$ for this investigation represents an actual ejector weight-flow ratio on the order of 0.20 with an afterburner operating at rated temperature.

Symbols, subscripts, and parameters used are defined in appendix A. Calculations and definitions used in presenting the data are the same as in reference 7, appendix B. The integrated thrust method is explained in appendix B of this report.

PRESENTATION OF DATA

Primary-Nozzle Performance

The primary thrust ratio and flow coefficient (defined in appendix A) with and without the shroud are shown in figures 4 and 5 as functions of primary pressure ratio for both primary nozzles. Thrust performance was practically the same for both nozzles within experimental accuracy; but, as expected, the flow coefficient was higher for the low-convergence-angle primary nozzle. The flow coefficient was unaffected by variations in the shroud length or ejector corrected weight-flow ratio.

Ejector Performance

The principal difference between fixed- and variable-shroud ejectors for supersonic aircraft is in their off-design performance. This difference is especially significant if there is a nonafterburning high subsonic cruise requirement that would necessitate a compromise of the fixed-shroud-ejector design-point performance. The compromise may be accomplished by: (1) decreasing the expansion ratio so that the jet would not be so overexpanded at off-design conditions, or (2) decreasing the shroud spacing ratio to induce off-design separation of the jet, thus resulting in essentially convergent nozzle performance. The latter effect could also be achieved by increasing the shroud divergence angle or by moving the primary nozzle downstream during the transition from afterburning to nonafterburning. As previously mentioned, it is the latter principle that was incorporated in the design of the ejectors investigated.

The performance is discussed in terms of an assumed engine operating schedule, given in figure 6, in order to show the variation of

performance with Mach number. The nozzle-pressure-ratio schedule shown is typical for Mach 2.2 aircraft, and the inlet recovery is based on a kinetic-energy efficiency of 0.95. Full afterburning is assumed for takeoff and acceleration to Mach 2.2 and nonafterburning for Mach 0.9 cruise. It is also assumed that no base or boattail pressure reduction took place at the ejector exit.

The thrust performance of the two ejectors investigated is presented in the data plots of figure 7, which give the ejector thrust ratio as a function of primary pressure ratio for several values of ejector corrected weight-flow ratio. The composite performance of the high-spacing-ratio ejector is presented in figure 8 as a function of Mach number. Inasmuch as the ejector thrust ratio includes isentropic or ideal thrust in the denominator, it is essentially a measure of jet expansion efficiency.

Nonafterburning thrust performance. - Nonafterburning thrust performance for spacing ratios of 1.05 and 1.24 is given in figures 7(a) and (b). The significant operating region for this condition corresponds to primary pressure ratios up to about 4.0. In this region, the thrust characteristics for both ejectors are similar to those of a convergent nozzle. For the shorter ejector, figure 7(a), thrust ratios of 0.974 and above were obtained for corrected ejector weight-flow ratios at zero and above. In general, as shown in figure 7(b), for the lower secondary flows increasing the spacing ratio from 1.05 to 1.24 induced the primary flow to attach at a lower primary pressure ratio with slightly greater attendant overexpansion losses. At a corrected ejector weight-flow ratio of 0.08, however, the performance recovered and was as good as for the shorter shroud. Both ejectors encountered hysteresis at zero-corrected ejector weight-flow ratio between primary pressure ratios of about 3.0 and 6.0.

If an aircraft using this ejector had low base or boattail pressure, the effective primary pressure ratio could be increased from 4.0 to as high as 6.0 or 7.0, and consequently ejector performance would not be as good. Thus, careful attention to the boattail fairing is essential for good internal performance as well as low external drag.

Afterburning thrust performance. - Afterburning thrust performance for spacing ratios of 1.01 and 1.15 is given in figures 7(c) and (d). The region of interest here extends from a primary pressure ratio of about 2.0 corresponding to takeoff to about 12.0 corresponding to operation at Mach 2.2. The thrust performance obtained is typical of that for divergent ejectors (ref. 7). For the shorter ejector, figure 7(c), ejector thrust ratios greater than 0.98 were obtained at a takeoff primary pressure ratio of 2.0 with ejector corrected weight-flow ratios above about 0.04. Peak thrust performance for this configuration (ejector thrust ratio of 0.99 or better) occurred very near the design

primary pressure ratio of about 10.7 with corrected ejector weight-flow ratios of 0.027 and higher. In general, from figure 7(d), increasing the spacing ratio from 1.01 to 1.15 increased the performance about 1.0 percent over the entire operating region except at primary pressure ratios near 2.0.

As previously indicated, if the nonafterburning configuration is not operated at too low an ejector corrected weight-flow ratio (above 0.08), its performance will be independent of shroud spacing; so that from a consideration of both afterburning and nonafterburning performance the large-spacing-ratio configuration would be a slightly better one.

Composite thrust performance. - Figure 8 shows the performance of the high-spacing-ratio ejector as a function of Mach number for conditions of the previously mentioned assumed operating schedule (fig. 6) with the assumption that the base pressure was equal to ambient.

As compared with a continuously variable ejector (ref. 10), the only region where thrust performance is compromised (ejector thrust ratios below 0.99) is in the Mach number region from 0.4 to 1.2, where the thrust ratio decreased to a minimum of 0.96. This overexpansion loss was limited to about 4 percent with the use of an ejector corrected weight-flow ratio of about 0.07. It appears that, on a gross thrust basis, internal performance in this region could be improved by using ejector corrected weight-flow ratios at the onset of afterburning acceleration that are even larger than those investigated.

Pumping performance. - Suitability of an ejector is not determined by thrust performance alone. It must also be capable of pumping adequate cooling air and matching inlet conditions.

Air-handling characteristics for all ejector configurations are shown in figure 9 by plots of ejector total-pressure ratio against primary pressure ratio for various ejector corrected weight-flow ratios. A line of the maximum ejector total-pressure ratio found from the assumed inlet and engine operating schedule and assumed secondary-duct subsonic pressure ratio of 0.95 is also included. This curve represents the limit of ejector operation using inlet duct air.

If inlet ram air were used, all of the ejector configurations investigated could easily supply any ejector corrected weight-flow ratio up to the maximum investigated at all primary pressure ratios except those corresponding to sea-level static operating conditions.

Integrated Thrust Performance

A comparison of the measured and integrated thrust values for the low-spacing-ratio configurations for selected ejector corrected weight-flow ratios is presented in figure 10 to determine the validity of such a method for application to full-scale in-flight thrust measurement. As in reference 9, which made the same comparison for lower divergence angles and expansion ratios, agreement was good with differences between measured and integrated values being, in general, within 1 percent. Much of this difference can be attributed to frictional forces that were not considered in the equation used.

SUMMARY OF RESULTS

A 0.278-scale internal-performance evaluation conducted on two fixed-divergent-shroud aircraft ejectors differing in shroud spacing ratio and designed for use in a Mach 2.2 aircraft indicated that:

1. If ejector corrected weight-flow ratios of the order of 0.10 are used, the performance of these fixed-geometry ejectors is, in general, as good as a continuously variable geometry ejector (ejector thrust ratio of about 0.99) except at conditions corresponding to afterburning acceleration from Mach 0.4 to 1.2, where the thrust ratio decreased to a minimum of about 0.96.

2. Increasing the ejector spacing ratio on the order of 16 percent did not affect the performance of the nonafterburning ejector at the high ejector weight-flow ratios (above 0.8) but improved the performance of the afterburning ejector about 1 percent.

3. Integrated and measured thrust values were, in general, found to agree within about 1 percent.

Lewis Research Center
National Aeronautics and Space Administration
Cleveland, Ohio, March 22, 1960

[redacted]

APPENDIX A

SYMBOLS

A	area, sq ft
C_d	flow coefficient, dimensionless
D	diameter, in.
F	gross thrust, lb
F_{ej}	measured ejector gross thrust, lb
$F_{ej,c}$	calculated ejector gross thrust, lb
g	gravitational constant, 32.174 ft/sec^2
L	spacing, in. (see fig. 1)
M	Mach number, dimensionless
m	mass flow, slugs/sec
P	total pressure, lb/sq ft abs
p	static pressure, lb/sq ft abs
R	gas constant, air, 53.3 ft-lb/(lb)($^\circ$R)
S	secondary gap height, ft (see fig. 1)
T	total temperature, $^\circ$R
V	velocity, ft/sec
w	weight flow, lb/sec
α	ejector flow angle, deg (see fig. 1)
γ	specific heat ratio (air), 1.4, dimensionless
θ	shroud divergence angle, deg (see fig. 1)

[redacted]

Subscripts:

b	base
d	divergent
e	exit
ip	ideal primary based on one-dimensional isentropic flow
is	ideal secondary based on one-dimensional isentropic flow
p	primary
s	secondary
0	ambient

Parameters:

D_e/D_p	shroud-exit diameter ratio
D_s/D_p	shroud-throat diameter ratio
$F_{ej}/(F_{ip} + F_{is})$	ejector thrust ratio
F_p/F_{ip}	primary thrust ratio
L/D_p	spacing ratio
P_p/p_0	primary pressure ratio
P_s/P_p	ejector total-pressure ratio
S/D_p	gap-length ratio
$(w_s/w_p)\sqrt{T_s/T_p}$	ejector corrected weight-flow ratio

[redacted]

APPENDIX B

INTEGRATED THRUST METHOD

The following describes the method of obtaining ejector thrust from pressure integrations and momentum forces. A control volume was chosen as shown by dotted lines:

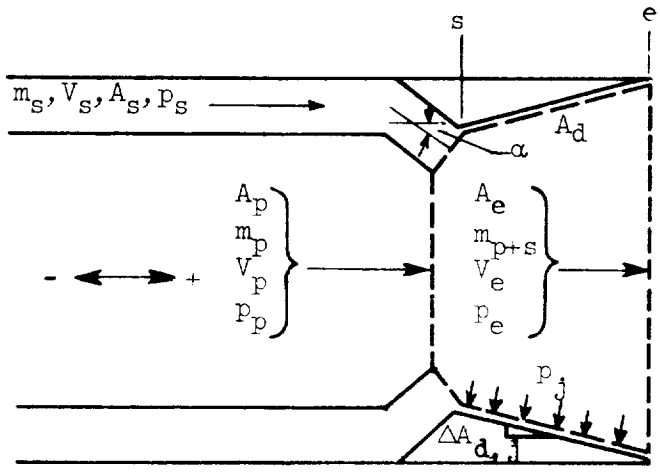

The equation governing the motion of the control volume is derived from Newton's second law and yields

$$F_{ej,c} = (m_p V_p + p_p A_p) + (m_s V_s \cos \alpha + p_s A_s) + \int_{A_s}^{A_e} p \, dA_d - p_0 A_e$$

The first term of the equation was obtained from the primary-nozzle thrust calibrations made prior to the ejector runs, since

$$m_p V_p + p_p A_p = F_p + p_0 A_p$$

where p_0 is measured without the shroud. The second term was evaluated according to

$$m_s V_s \cos \alpha + p_s A_s = m_s \cos \alpha \sqrt{\frac{2\gamma g R T_s}{\gamma - 1}\left[1 - \left(\frac{p_s}{P_s}\right)^{\frac{\gamma-1}{\gamma}}\right]} + p_s A_s$$

[redacted]

where $A_s = \pi(D_s^2 - D_p^2)/4$. The integration of the pressure along the divergent wall was approximated by a summation of area steps, which gave

$$\int_{A_s}^{A_e} p \, dA_d = \sum_{j=1}^{k} p_j \, \Delta A_j$$

where A_d is the vertical projected area of the divergent wall and p_j is the average static pressure of diametrically opposed wall taps. Since the wall static-pressure taps were located on equal projected incremental areas, the integral reduces as:

$$\int_{A_s}^{A_e} p \, dA_d = \Delta A_d \sum_{j=1}^{k} p_j; \qquad k \, \Delta A_d = A_d$$

$$= \frac{A_d}{k} \sum_{j=1}^{k} p_j; \qquad \bar{p}_d = \frac{\sum_{j=1}^{k} p_j}{k}$$

$$= \bar{p}_d A_d$$

where $\bar{p}_d$ is the arithmetical average static pressure acting on the divergent wall.

REFERENCES

1. Greathouse, W. K., and Hollister, D. P.: Air-Flow and Thrust Characteristics of Several Cylindrical Cooling-Air Ejectors with a Primary to Secondary Temperature Ratio of 1.0. NACA RM E52L24, 1953.

2. Greathouse, W. K., and Hollister, D. P.: Preliminary Air-Flow and Thrust Calibrations of Several Conical Cooling-Air Ejectors with a Primary to Secondary Temperature Ratio of 1.0. I - Diameter Ratios of 1.21 and 1.10. NACA RM E52E21, 1952.

3. Greathouse, W. K., and Hollister, D. P.: Preliminary Air-Flow and Thrust Calibrations of Several Conical Cooling-Air Ejectors with a Primary to Secondary Temperature Ratio of 1.0. II - Diameter Ratios of 1.06 and 1.40. NACA RM E52F26, 1952.

4. Allen, John L.: Pumping Characteristics for Several Simulated Variable-Geometry Ejectors with Hot and Cold Primary Flow. NACA RM E54G15, 1954.

5. Hearth, Donald P., and Valerino, Alfred S.: Thrust and Pumping Characteristics of a Series of Ejector-Type Exhaust Nozzles at Subsonic and Supersonic Flight Speeds. NACA RM E54H19, 1954.

6. Beheim, Milton A.: Off-Design Performance of Divergent Ejectors. NACA RM E58G10a, 1958.

7. Trout, Arthur M., Papell, S. Stephen, and Povolny, John H.: Internal Performance of Several Divergent-Shroud Ejector Nozzles with High Divergence Angles. NACA RM E57F13, 1957.

8. Greathouse, William K., and Beale, William T.: Performance Characteristics of Several Divergent-Shroud Aircraft Ejectors. NACA RM E55G21a, 1955.

9. Huntley, S. C., and Yanowitz, Herbert: Pumping and Thrust Characteristics of Several Divergent Cooling-Air Ejectors and Comparison of Performance with Conical and Cylindrical Ejectors. NACA RM E53J13, 1954.

10. Stofan, Andrew J., and Mihaloew, James R.: Performance of a Variable Divergent-Shroud Ejector Nozzle Designed for Flight Mach Numbers up to 3.0. NASA TM X-255, 1960.

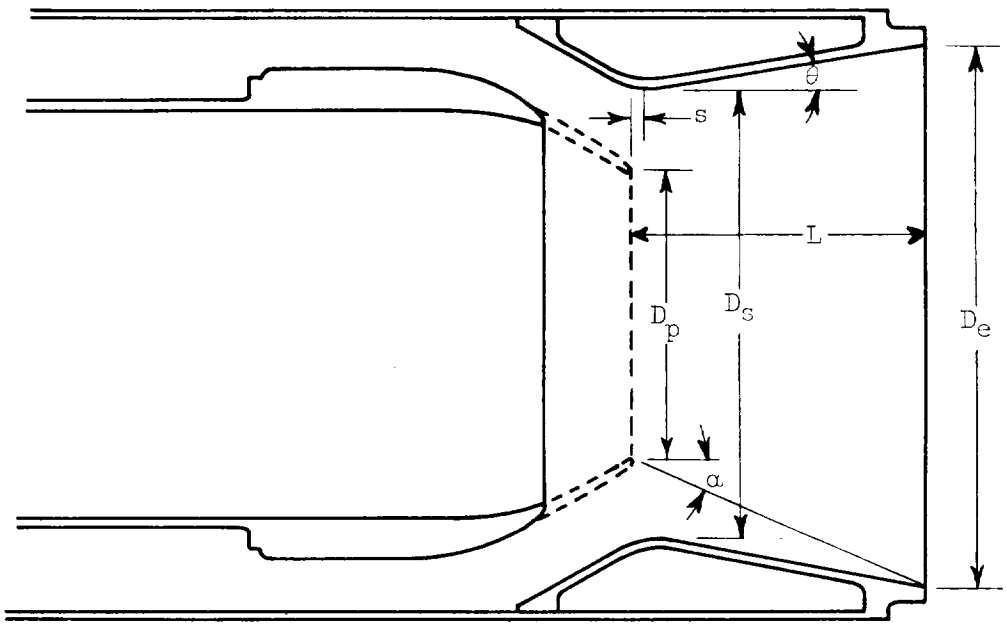

Configuration	D_p, in.	$\frac{D_e}{D_p}$	$\frac{D_s}{D_p}$	$\frac{L}{D_p}$	$\frac{S}{D_p}$	θ, deg	α, deg
Nonafterburning	7.31	1.84	1.52	1.05	0.096	10	21.8
Nonafterburning modified	7.31	1.84	1.52	1.24	.28	10	18.7
Afterburning	9.59	1.40	1.16	1.01	.28	10	11.2
Afterburning modified	9.59	1.40	1.16	1.15	.42	10	9.9

Figure 1. - Ejector geometry.

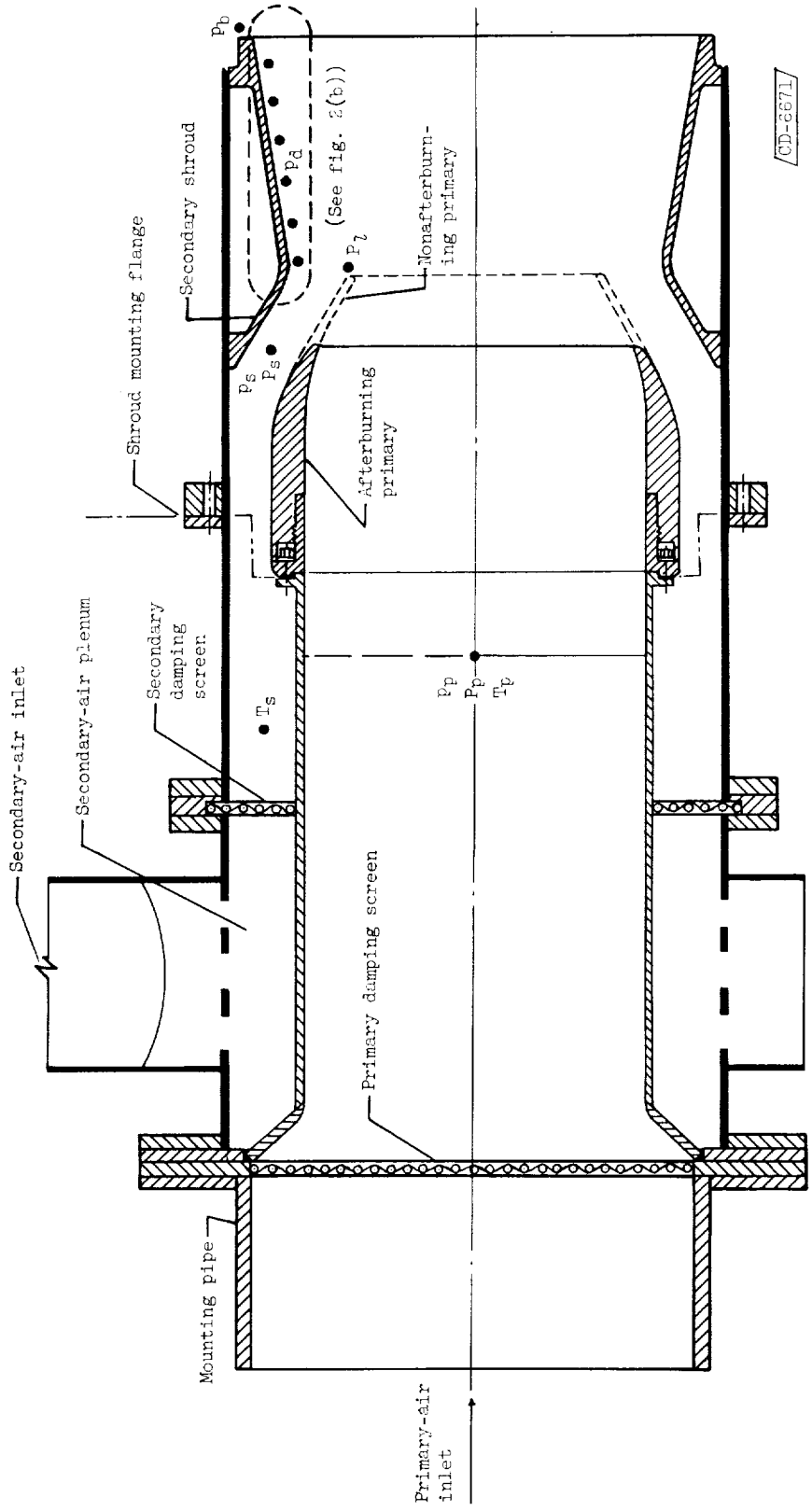

(a) Schematic drawing with instrumentation locations.

Figure 2. - Ejector installation and instrumentation.

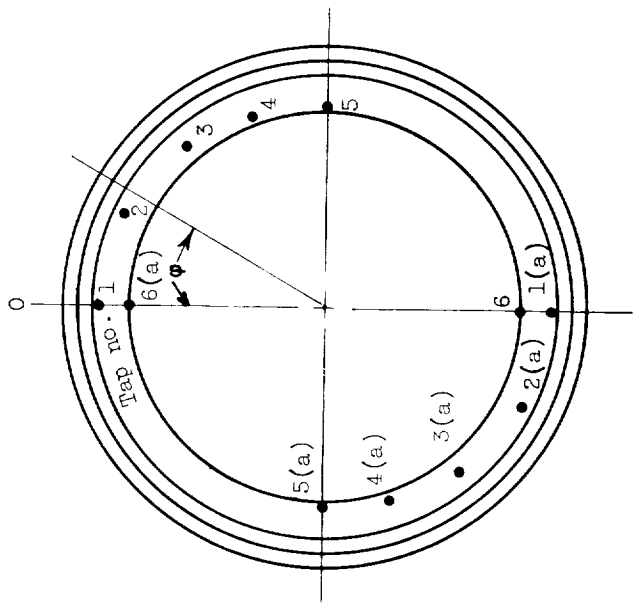

Tap	x, in.	φ, deg
1,1(a)	0.62	0, 180
2,2(a)	1.89	22.5, 202.5
3,3(a)	3.20	45, 225
4,4(a)	4.56	67.5, 247.5
5,5(a)	5.98	90, 270
6,6(a)	6.85	180, 0

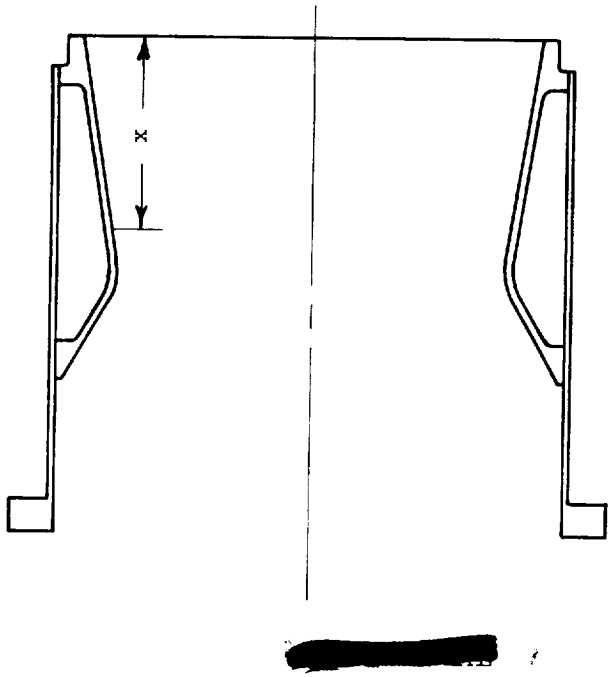

(b) Location of static-pressure taps on divergent shroud.

Figure 2. - Concluded. Ejector installation and instrumentation.

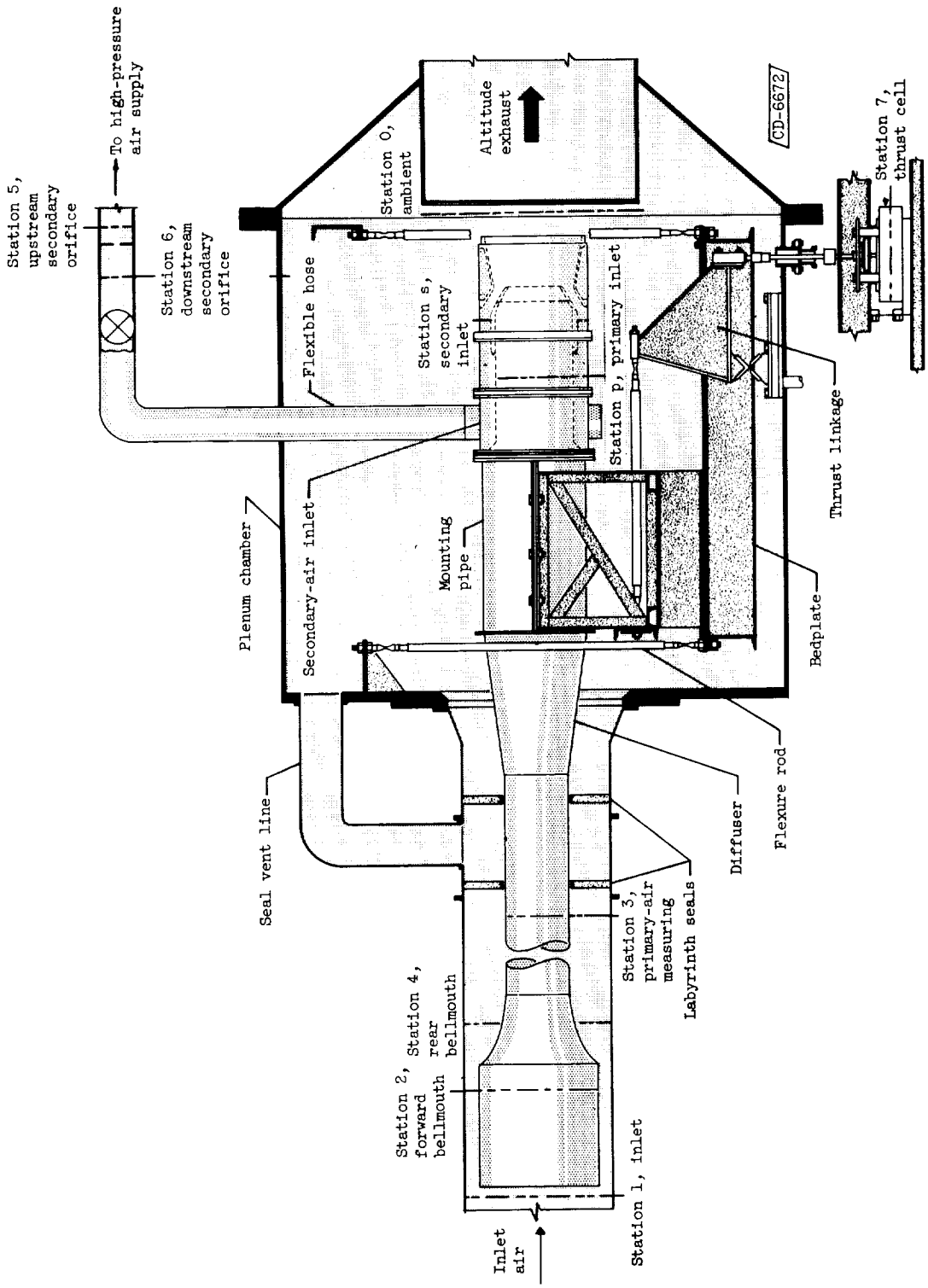

Figure 3. - Test setup and station locations.

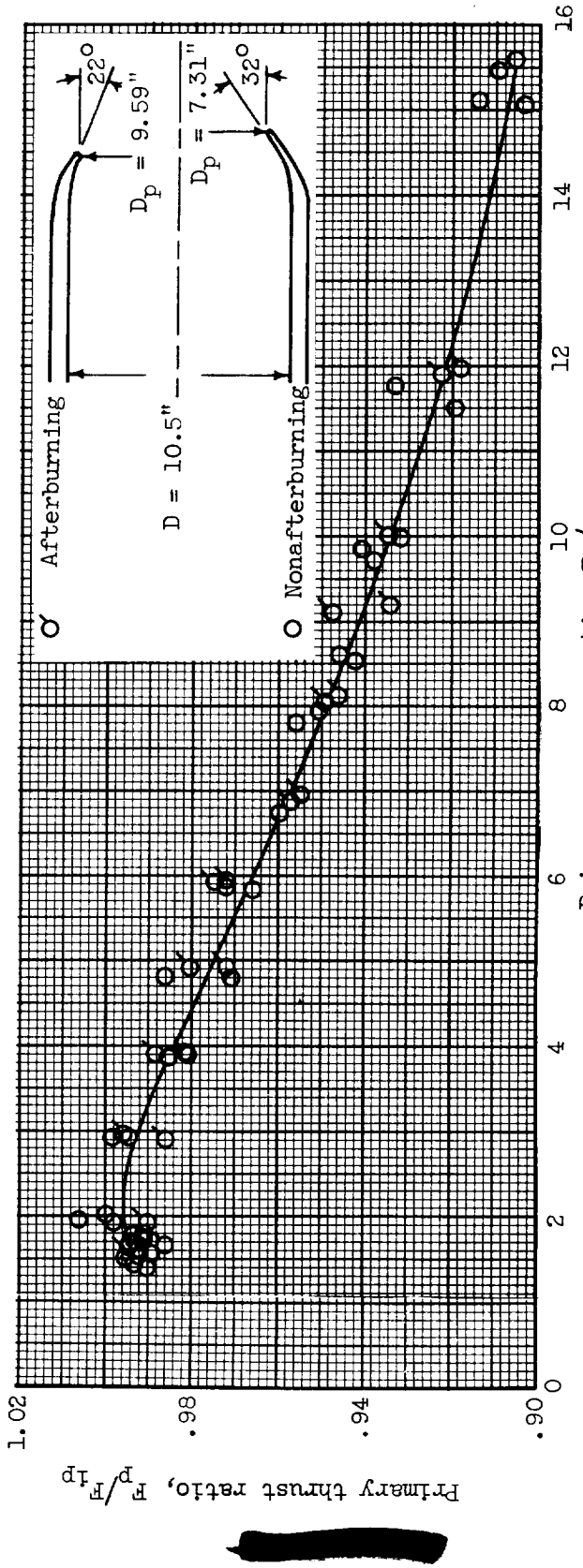

Figure 4. - Primary-nozzle thrust performance.

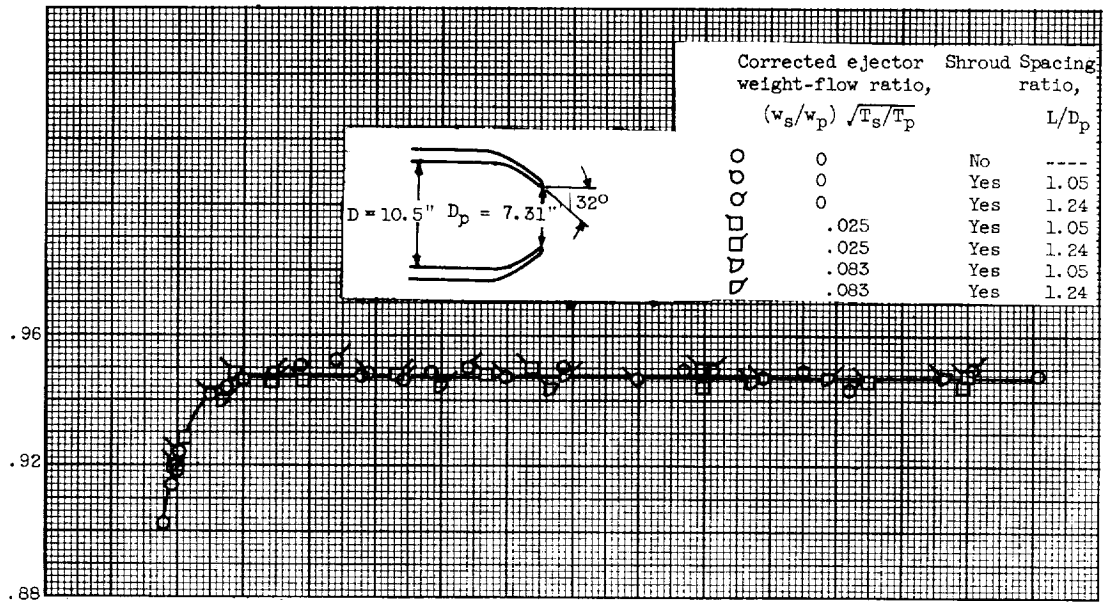

(a) Nonafterburning.

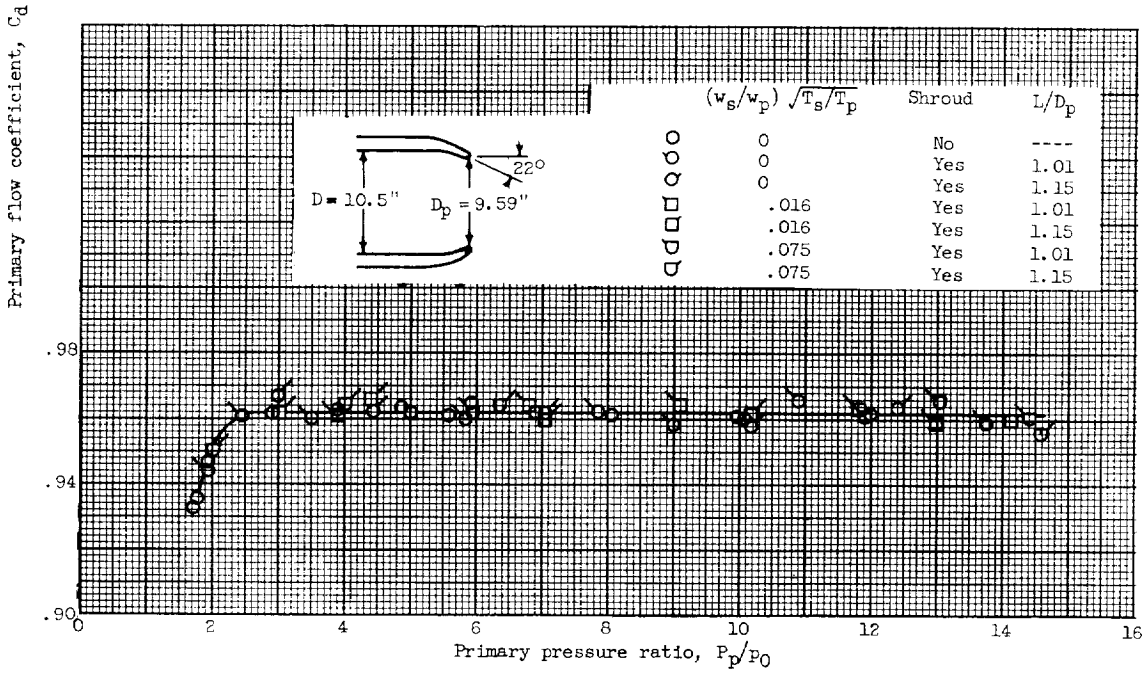

(b) Afterburning.

Figure 5. - Primary-nozzle flow performance.

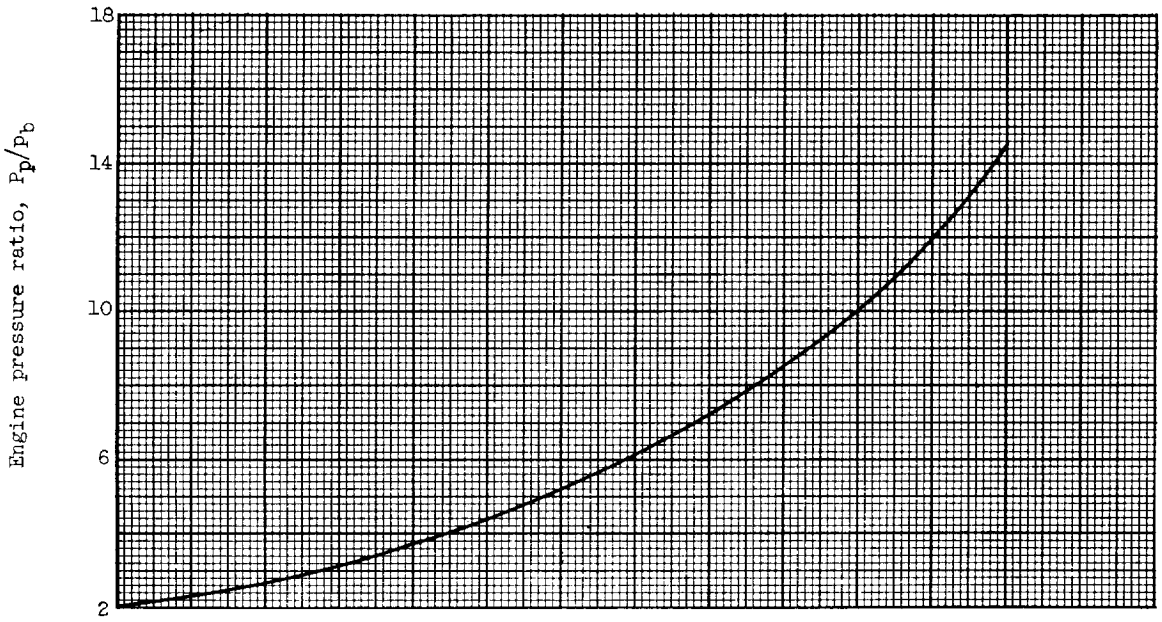

(a) Nozzle operating schedule.

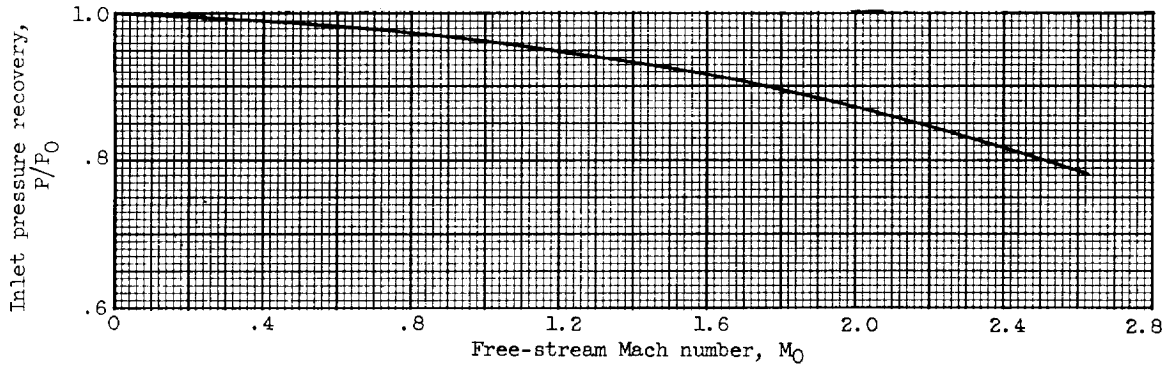

(b) Inlet recovery.

Figure 6. - Assumed engine operating schedule.

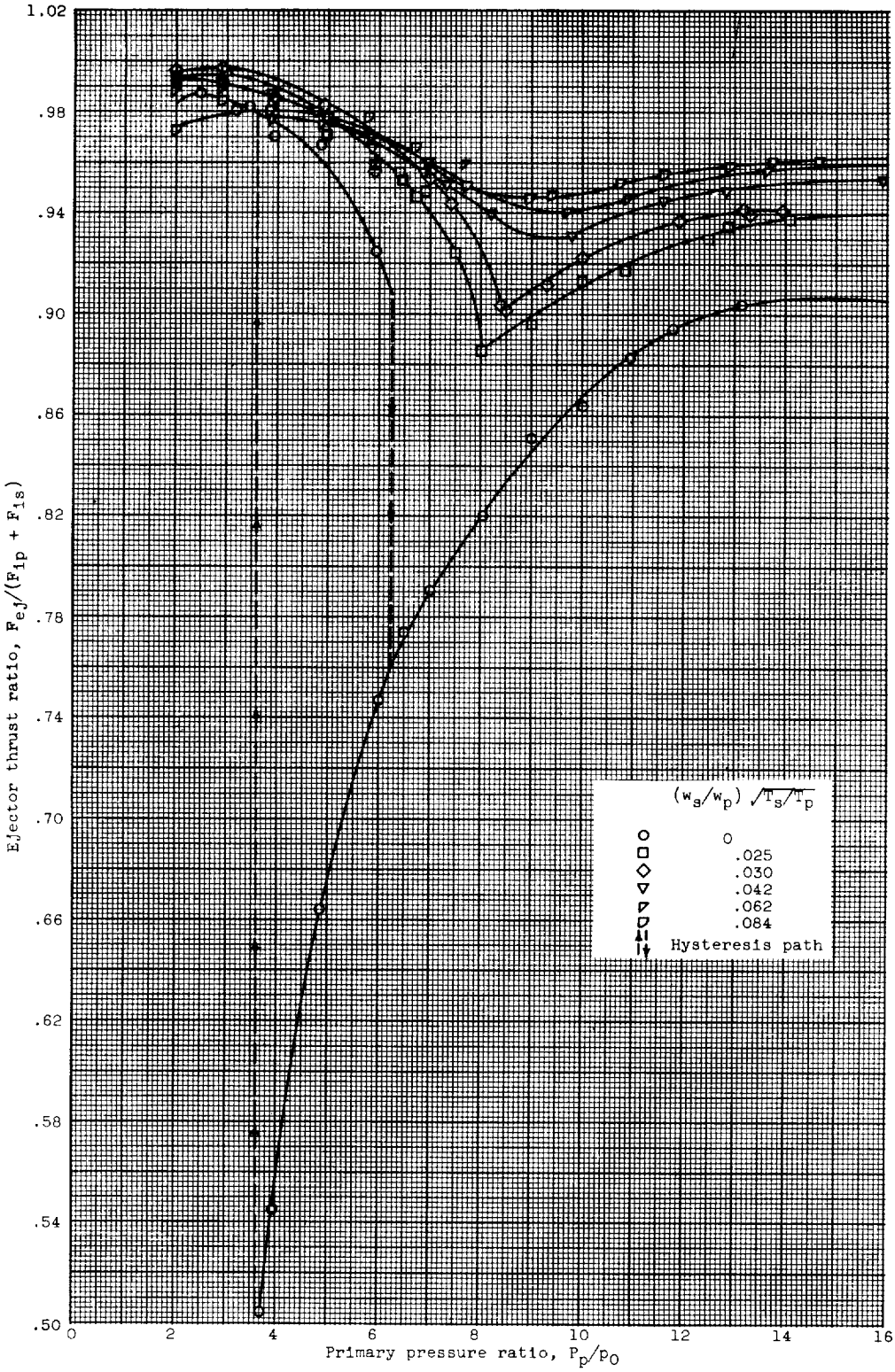

(a) Nonafterburning; L/D_p, 1.05.

Figure 7. - Ejector thrust performance.

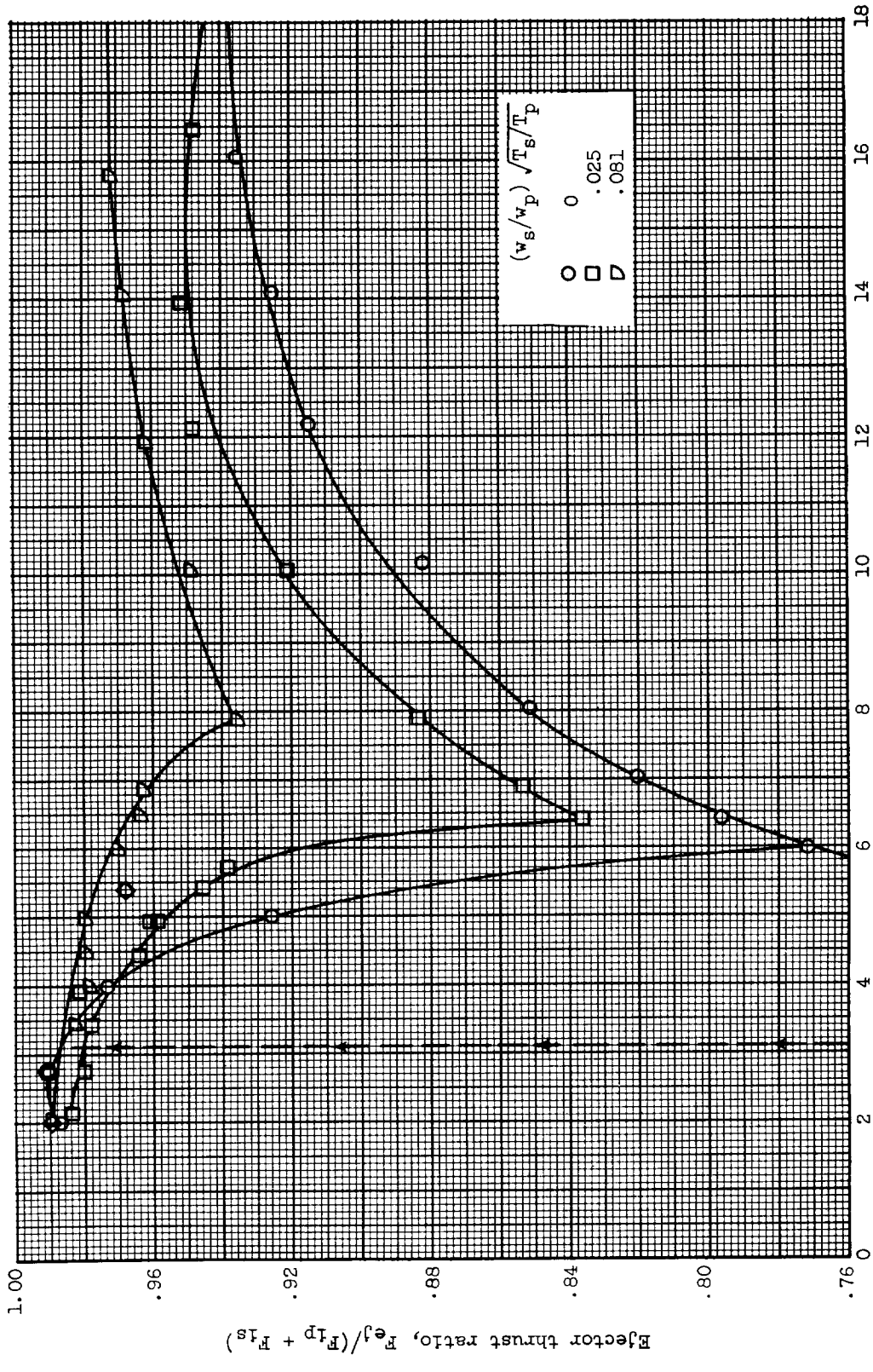

(b) Nonafterburning; L/D_p, 1.24.

Figure 7. - Continued. Ejector thrust performance.

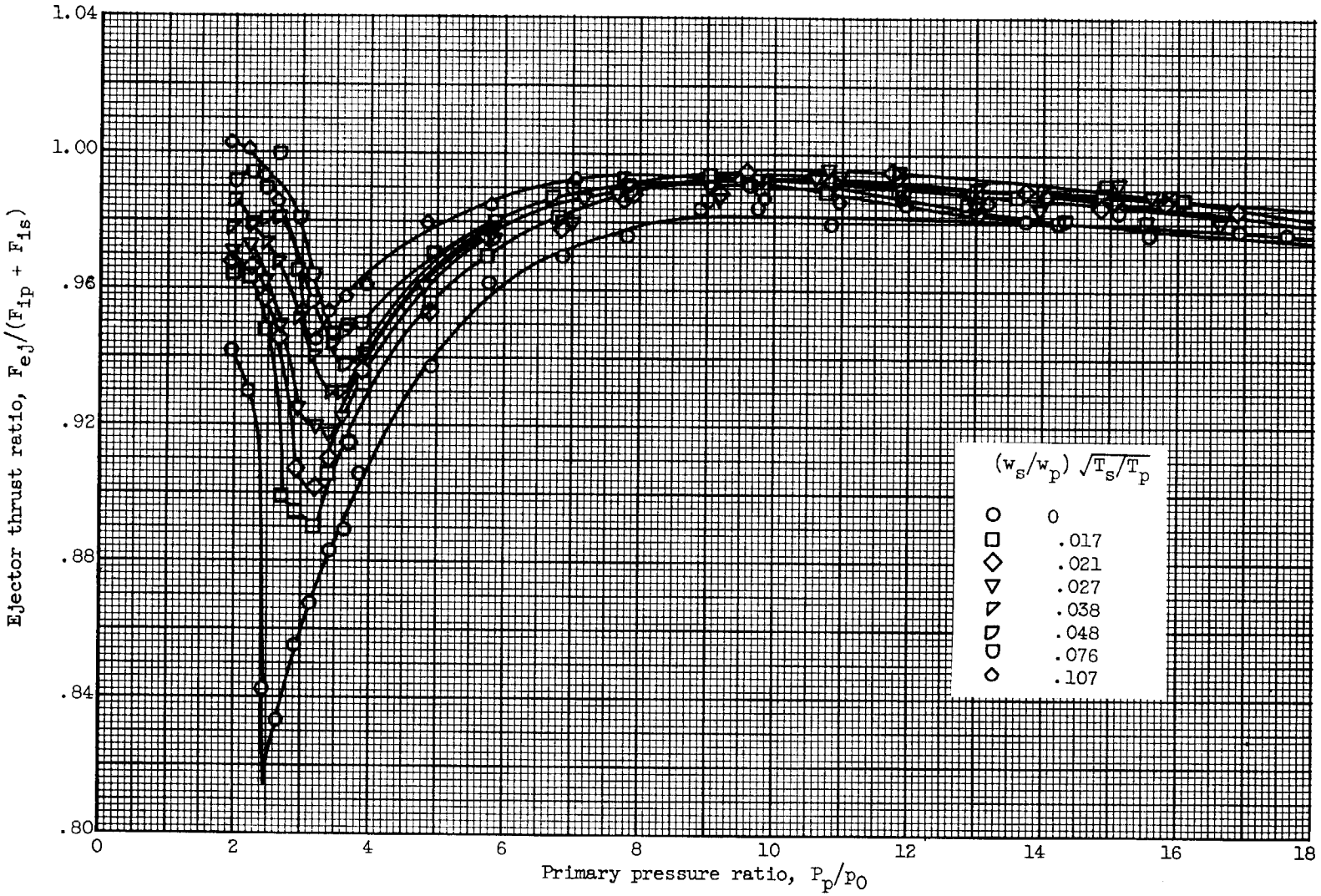

(c) Afterburning; L/D_p, 1.01.

Figure 7. - Continued. Ejector thrust performance.

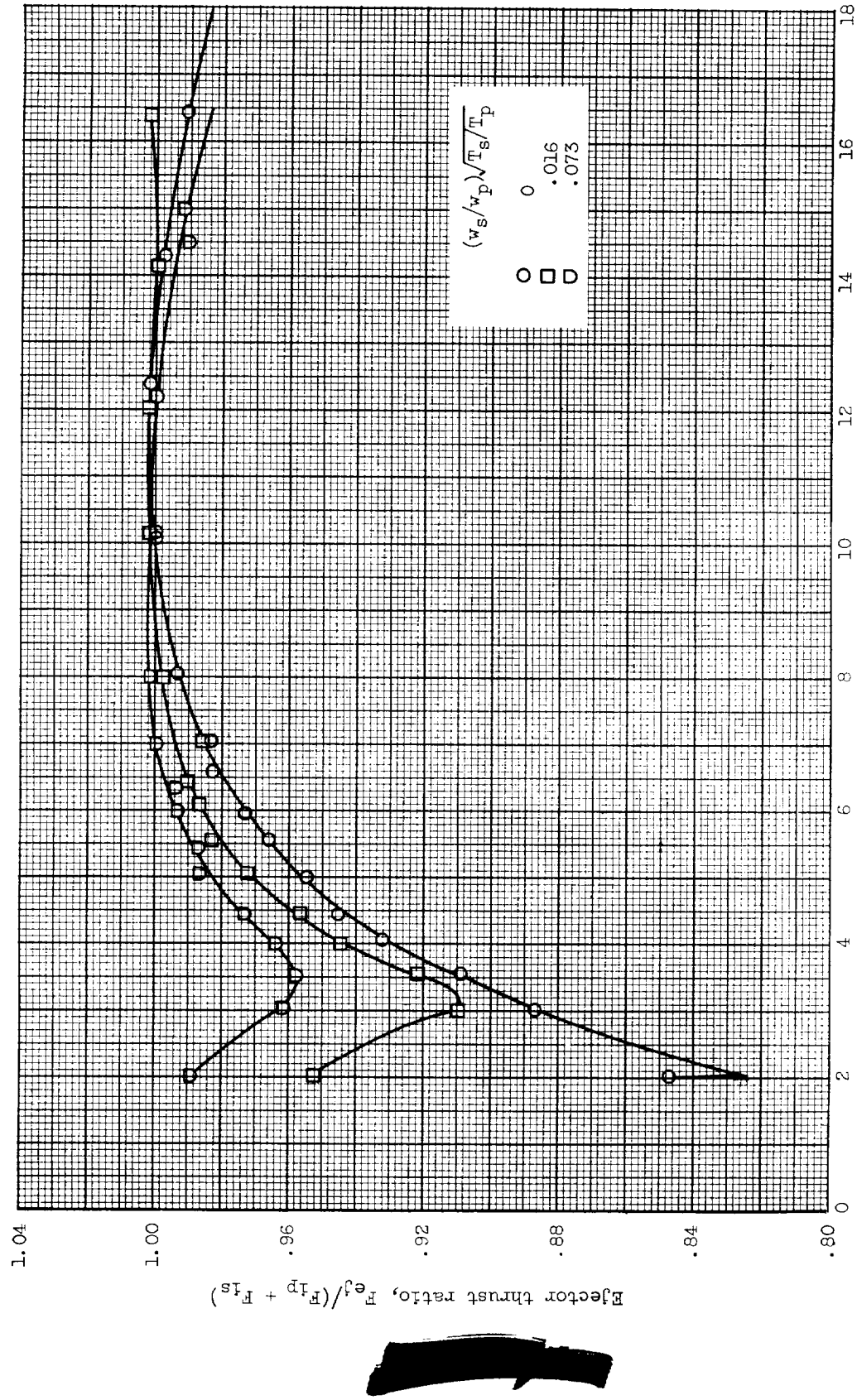

(d) Afterburning; L/D_p, 1.15.

Figure 7. - Concluded. Ejector thrust performance.

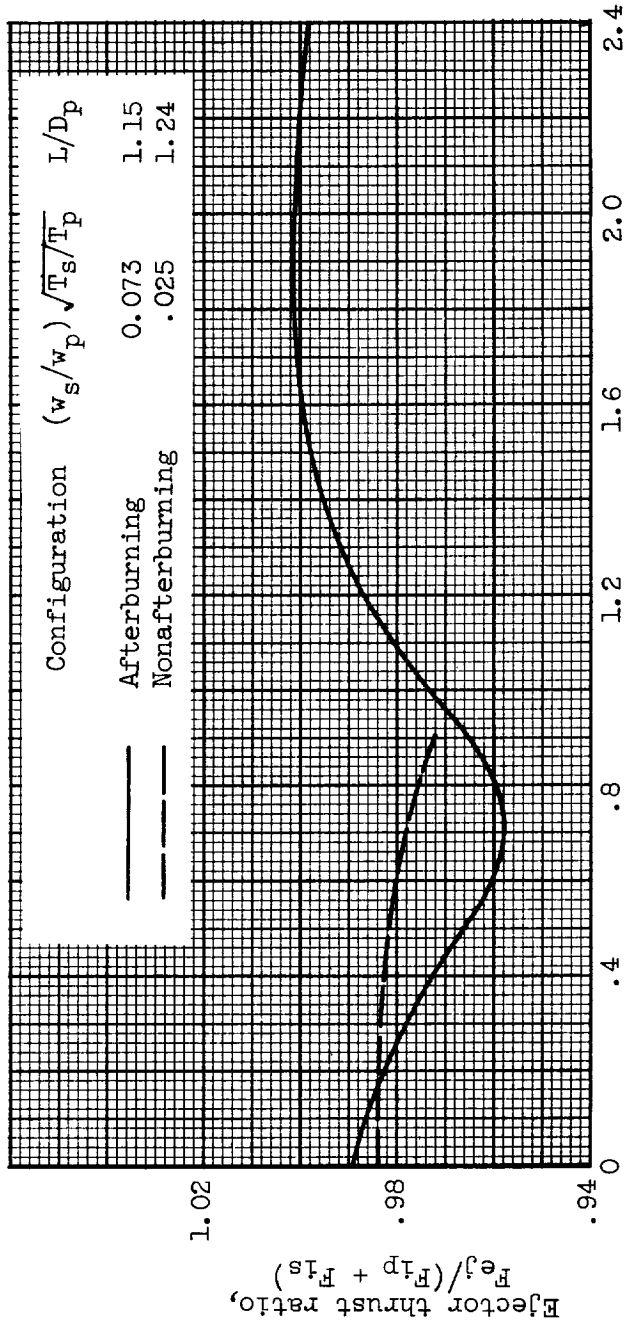

Figure 8. - Composite ejector thrust performance.

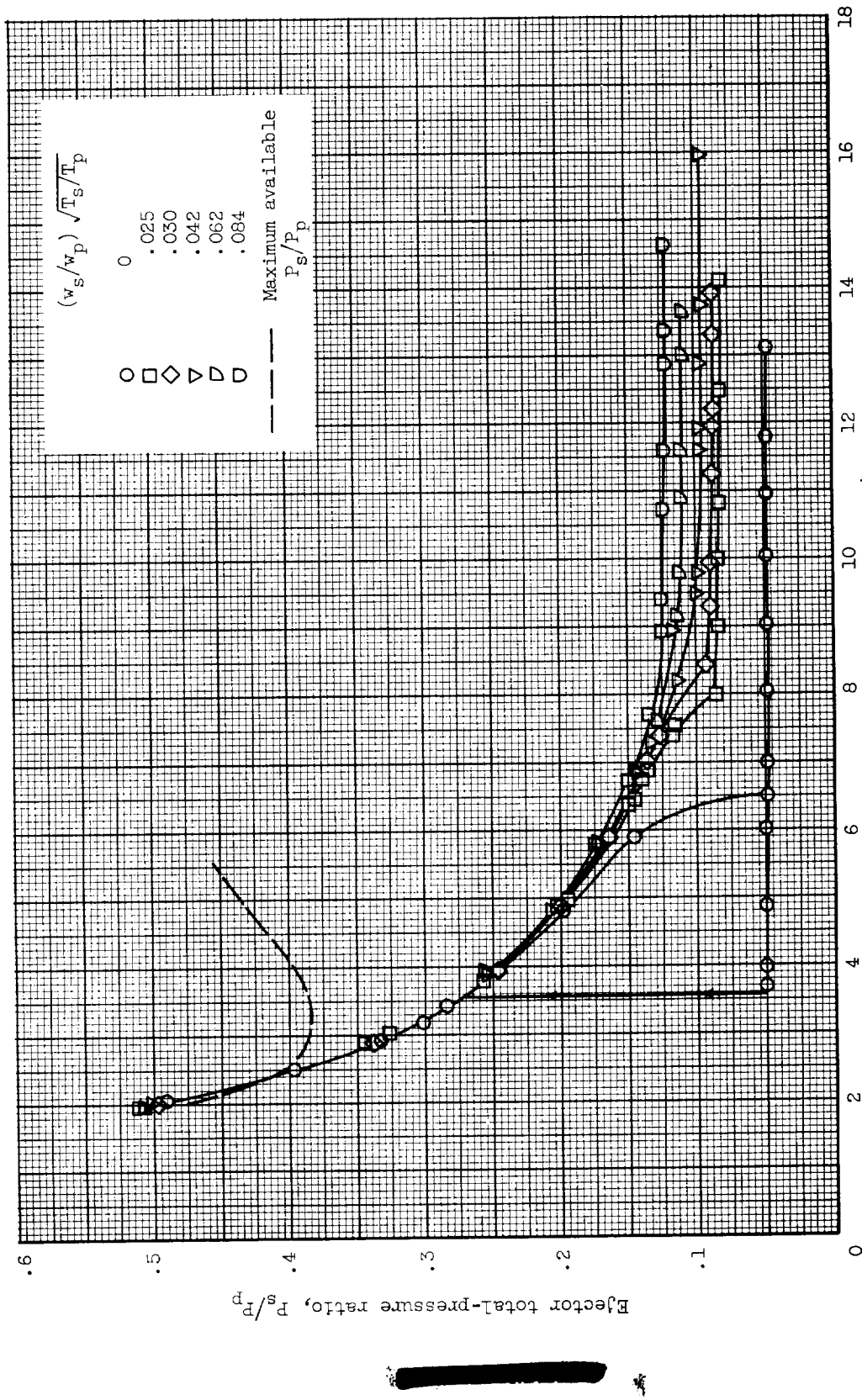

(a) Nonafterburning; L/D_p, 1.05.

Figure 9. - Ejector pumping performance.

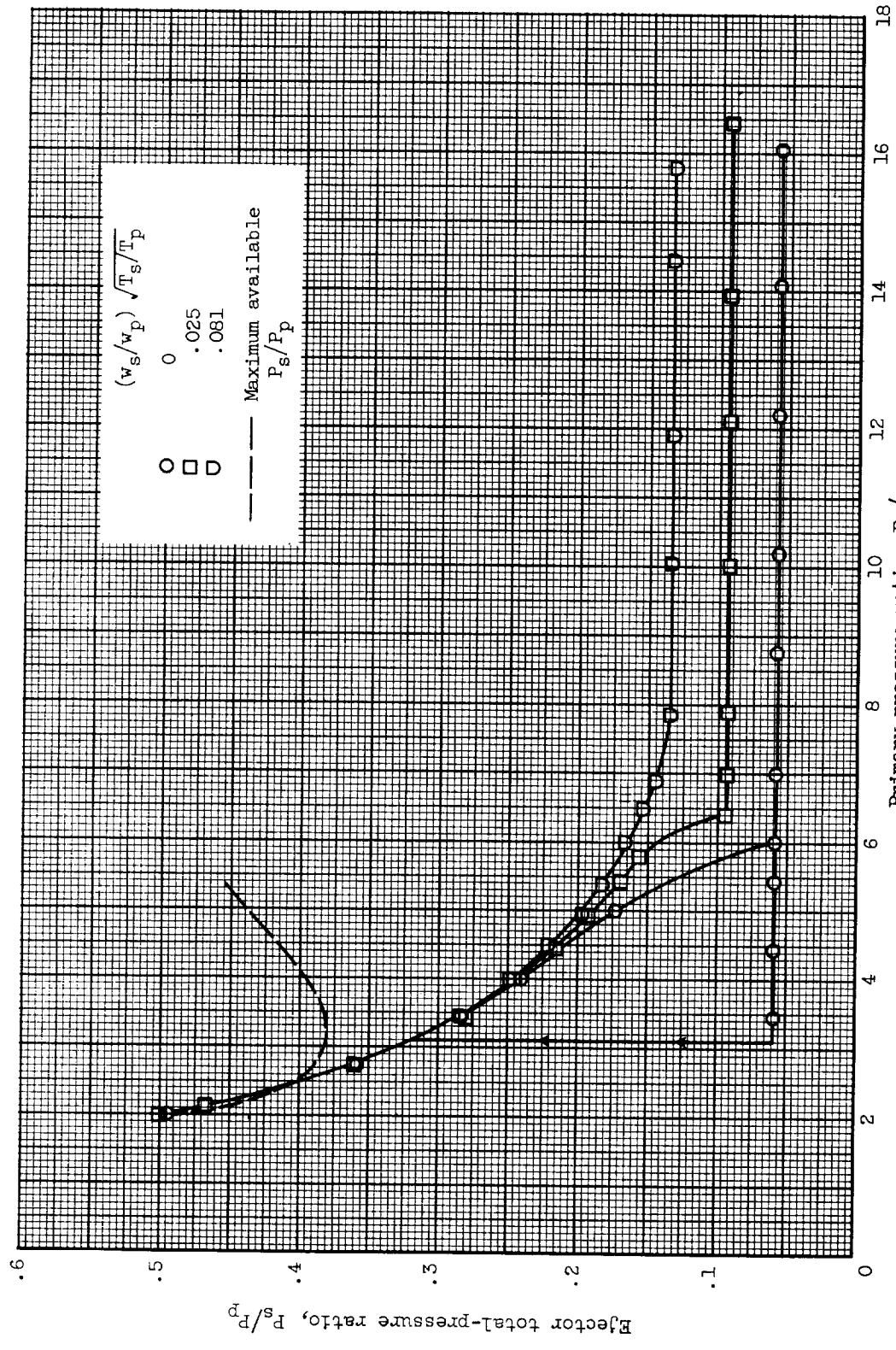

(b) Nonafterburning; L/D_p, 1.24.

Figure 9. - Continued. Ejector pumping performance.

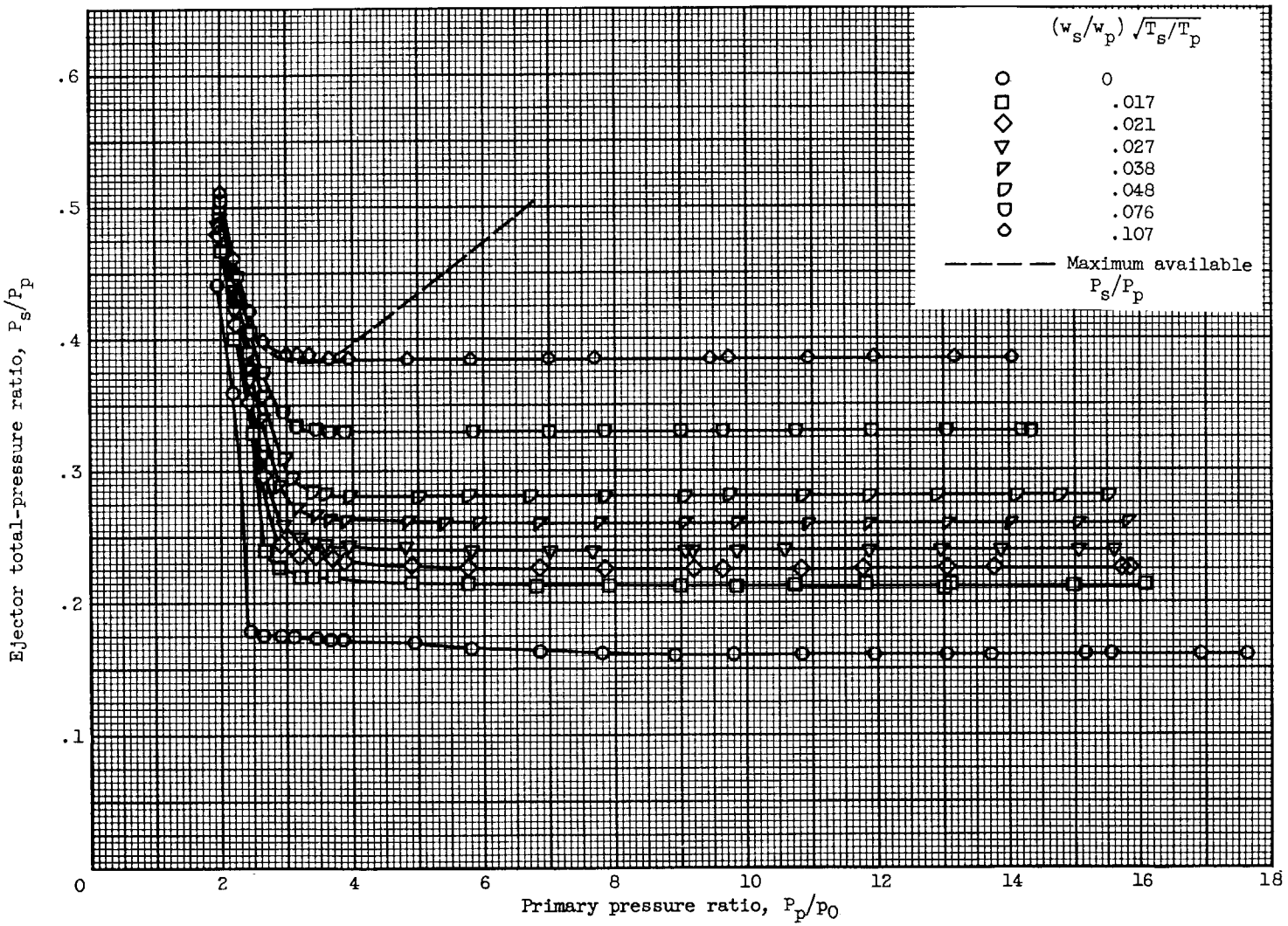

(c) Afterburning; L/D_p, 1.01.

Figure 9. - Continued. Ejector pumping performance.

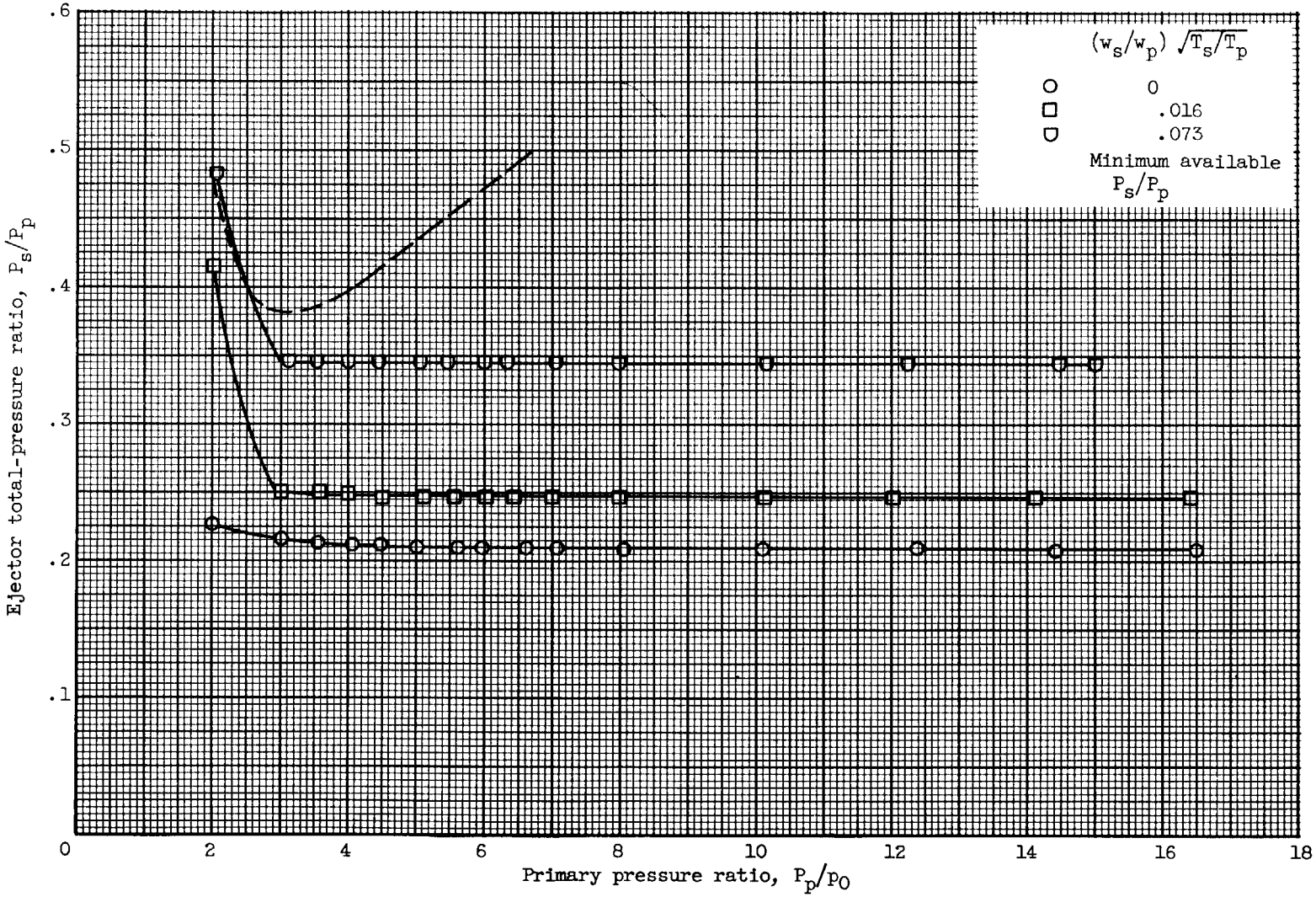

(d) Afterburning; L/D, 1.15.

Figure 9. - Concluded. Ejector pumping performance.

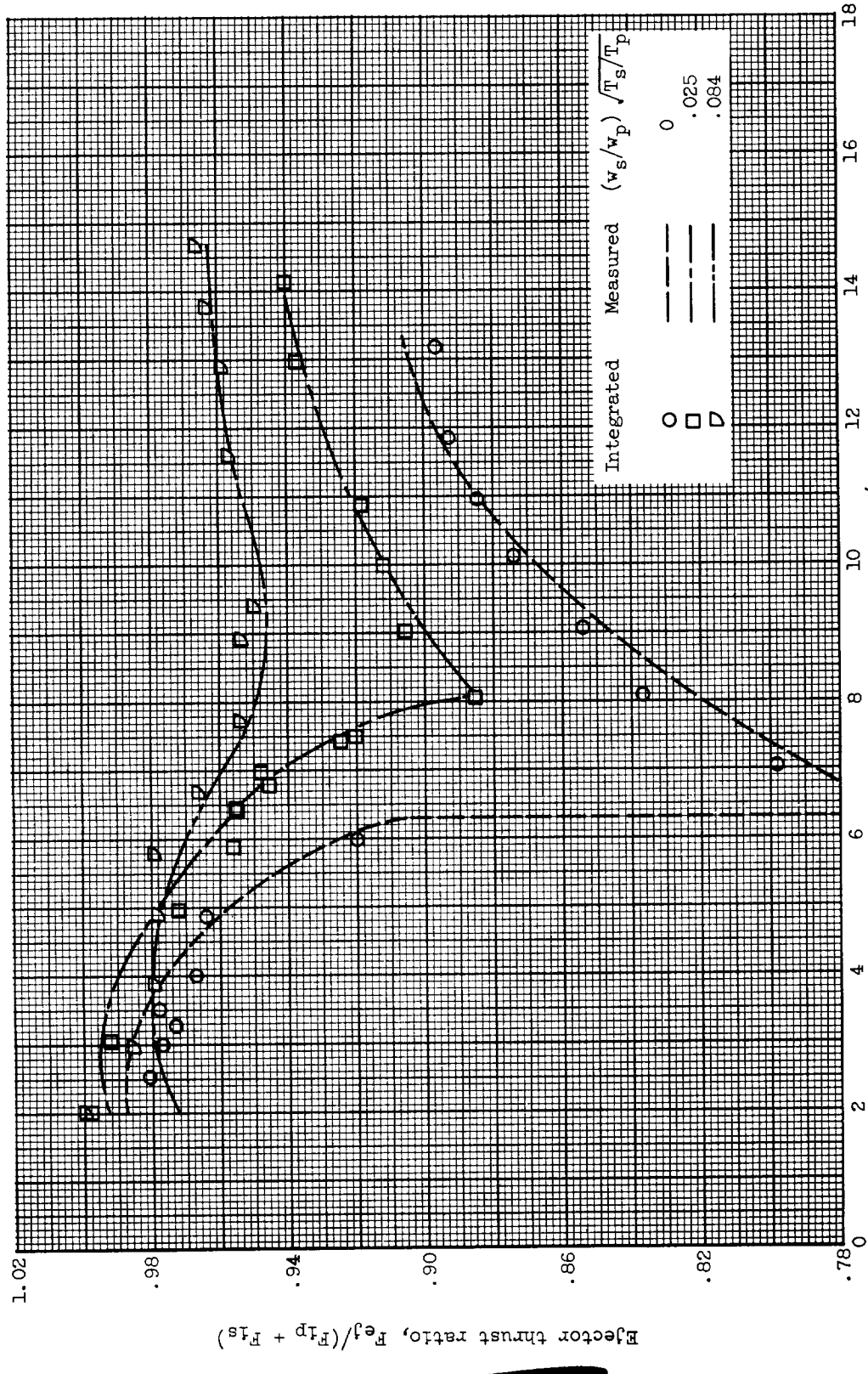

(a) Nonafterburning; L/D_p, 1.05.

Figure 10. - Comparison of integrated and measured thrust.

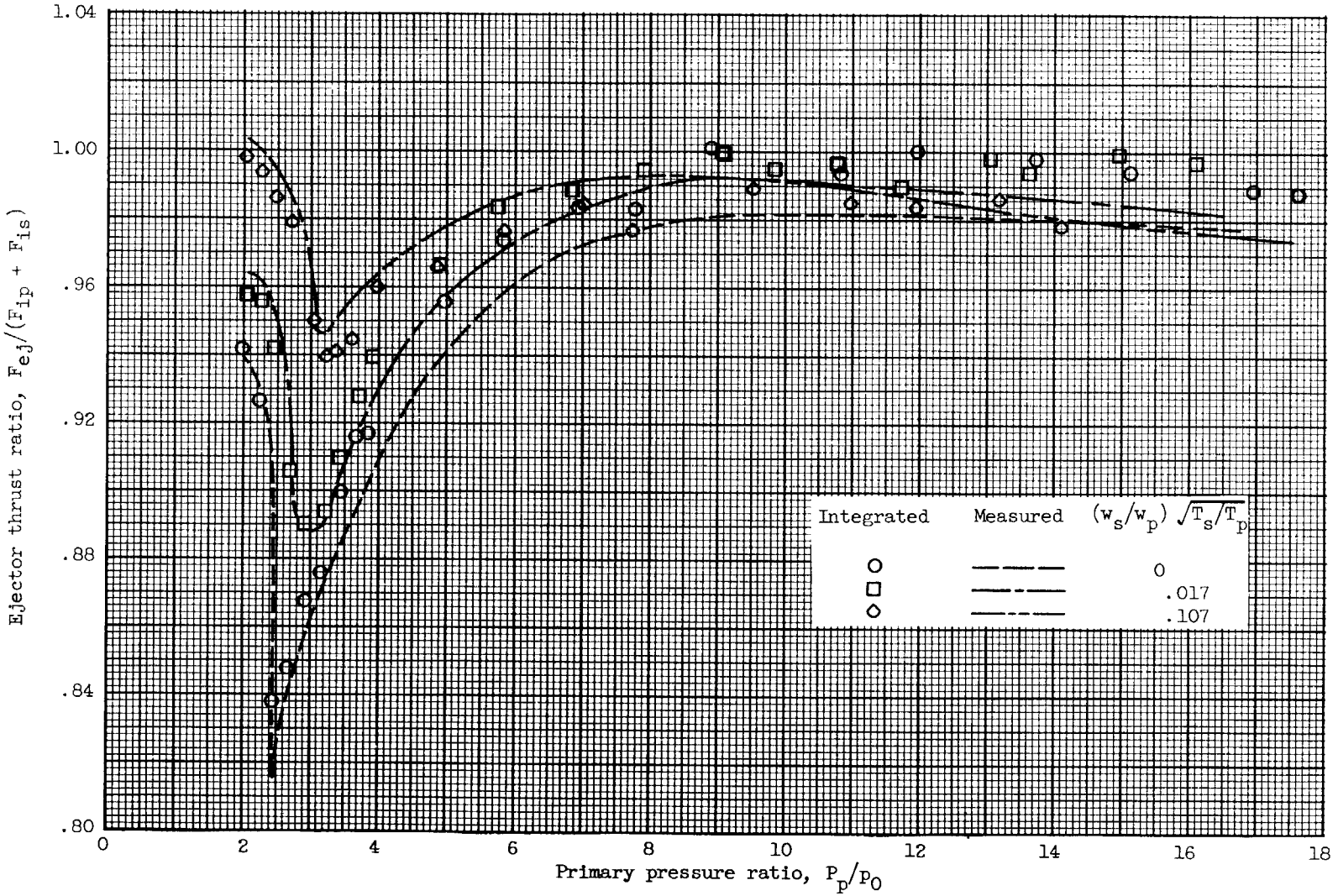

(b) Afterburning; L/D_p, 1.01.

Figure 10. - Concluded. Comparison of integrated and measured thrust.